TMS 2012

141st Annual Meeting & Exhibition

Supplemental Proceedings

Volume 1: Materials Processing and Interfaces

WILEY

TMS

TMS2012

141st Annual Meeting & Exhibition

Supplemental Proceedings

Volume 1: Materials Processing and Interfaces

TMS2012

141st Annual Meeting & Exhibition

Supplemental Proceedings

Volume 1: Materials Processing and Interfaces

About this volume

The *TMS 2012 Annual Meeting Supplemental Proceedings, Volume 1: Materials Processing and Interfaces*, is a collection of papers from the 2012 TMS Annual Meeting and Exhibition, held March11–March 15, in Orlando, California, U.S.A.

The papers in this volume were selected based on technical topic compatibility and represent ten symposia from the meeting. This volume, along with the other proceedings volumes published for the meeting, and archival journals, such as *Metallurgical and Materials Transactions* and *the Journal of Electronic Materials*, represents the available written record of the 65 symposia held at the 2012 TMS Annual Meeting.

The individual papers presented within this proceedings volume have not necessarily been edited or reviewed by the conference program organizers and are presented "as is." The opinions and statements expressed within the papers are those of the individual authors only and are not necessarily those of anyone else associated with the proceedings volume, the source conference, or TMS. No confirmations or endorsements are intended or implied.

WILEY

A John Wiley & Sons, Inc., Publication

TMS

Published by John Wiley & Sons, Inc., Hoboken, New Jersey.
Published simultaneously in Canada.

Library of Congress Cataloging-in-Publication Data is available.

ISBN 978-1-11829-607-3

Printed in the United States of America.

10 9 8 7 6 5 4 3 2 1

WILEY

A John Wiley & Sons, Inc., Publication

TMS

TABLE OF CONTENTS
Supplemental Proceedings: Volume I: Materials Processing and Interfaces

Advances in Surface Engineering: Alloyed and Composite Coatings

Session II

Session III

Session IV

Session V

General Poster Session

Session I

Mechanical Behavior Related to Interface Physics

Grain Boundaries: Experiment and Modeling

Interface Evolution under Mechanical Loading: Experiment, Characterization, and Theoretical Modeling

Interface Structures: Characterization, Theory, and Modeling

Poster Session

Nanocomposites

Mechanical Behavior and Modelling of Nanocomposites

Processing of Nanocomposites I

Nanocomposites for Magnetic and Dielectric Applications

Nanocomposite Interfaces and Characterization

Processing of Nanocomposites II

Poster Session

New Advances in Synthesis, Characterization, and Application of Layered Double Hydroxides

Session I

Randall M. German Honorary Symposium on Sintering and Powder-Based Materials

Sintering Theory and Practice

Current Activated and Conventional Sintering

Powder Technology

Powder Processing and Consolidation I

Powder Processing and Consolidation II

Powder Processing and Consolidation III

Recent Developments in Biological, Electronic, Functional and Structural Thin Films and Coatings

Process-Properties-Performance Correlations I

Process-Properties-Performance Correlations II

Applications to Bio, Energy and Electronic Systems

Process-Properties-Performance Correlations III

Science and Engineering of Light Metal Matrix Nanocomposites and Composites

Metal Matrix Nanocomposites

Nanocomposites and Composites

Metal Matrix Composites

Titanium: Advances in Processing, Characterization and Properties

Processing and Process Modeling I

Processing and Process Modeling II

Microstructure Evolution and Characterization I

Mechanical Properties

General Abstracts

Wettability and Interfacial Phenomena between Metals and Ceramic/Refractory Materials

Session I

TMS2011 General Abstracts: Structural Materials Division

Microstructure

TMS2012

141st Annual Meeting & Exhibition

Advances in Surface Engineering: Alloyed and Composite Coatings

STRUCTURAL COATINGS IN ALUMINUM ALLOY MICROTRUSS MATERIALS

Bosco Yu, Glenn D. Hibbard

Department of Materials Science and Engineering, University of Toronto,
184 College Street, Toronto, Ont., M5S 3E4, Canada

Keywords: Surface Engineering, Aluminum, Microtrusses, Energy Absorption

Abstract

Incorporating an internal cellular architecture of open space is one strategy to increase the potential functionality of aluminum alloys. Stretch-dominated microtruss cellular architectures, which are designed such that externally applied loads are resolved axially along the internal struts, provide enhanced strength and stiffness at low densities when compared to conventional metal foams. In this study we introduce the idea of using a structural coating to reinforce AA3003 aluminum alloy microtrusses. Because the internal surface area is large and the strut cross-sectional dimensions can be as small as hundreds of microns, only a 40 μm thick hard anodized alumina coating was needed to induce a four-fold increase in compressive strength and a six-fold increase in energy absorption at virtually no additional weight penalty. Backscatter electron microscopy was used to examine the failure mechanisms of the structural coatings and the cores in order to explain such a large change in behaviour.

Introduction

Microtrusses cellular materials have attracted considerable interest because of their structural efficiency and their potential to exhibit multifunctional characteristics [1-10]. In term of load bearing capacity, microtrusses are designed with a high degree of internal strut connectivity. Externally applied loads are resolved by axial (stretching) rather than bending deformation, making them up to ten times stiffer and three times stronger than conventional metal foams at low relativity densities [11]. Since the internal surface areas are large and the strut cross-sections are small, surface modification can also be used to further enhance their mechanical behaviour. Recently, electrodeposition of a ~50μm thick coating of ultrahigh strength nanocrystalline nickel was found to double and triple the compressive strength of low carbon steel and aluminum microtrusses, respectively [5, 6, 12].

Inelastic buckling was the overall failure mechanism seen for both conventional and structurally coated microtrusses [6]. Under this failure mechanism, the load carrying capacity of the microtruss progressively decreases making these materials less desirable for energy absorption applications. A recently study, however, indicated the possibility of enhancing the energy absorption behaviour of aluminum microtrusses by applying anodic oxide coating in order to change their overall collapse mechanism from inelastic buckling to hinge rotation and fracture [13]. The present study examines this hinge rotation and fracture failure mechanism in order to understand the mechanism of enhanced energy absorption in anodized microtruss materials.

Experimental

AA3003 aluminum perforated sheets (sheet thickness of 0.74 ± 0.01 mm) were purchased from McNichols Perforated Products (Altanta, GA). The perforation pattern had square holes of 5.10×5.10 mm punched on a square lattice of 6.36×6.36 mm creating an open area fraction of Φ = 0.64; Fig. 1a shows a schematic diagram of the starting sheet materials. The aluminum sheets were annealed at 600 °C for 30 minutes and then water cooled before forming into pyramidal microtrusses, after Bouwhuis et al. [5, 14]. Three forming/annealing cycles (with intermediate annealing treatments of 600 °C for 30 minutes) were used to achieve an internal truss angle of θ = 42.6° ± 0.1° and a relative density of $\bar{\rho}$ = 4.8% (in Fig. 1b). The microtrusses were subsequently given a post-fabrication annealing treatment of 600 °C for 30 minutes to remove any fabrication-induced work hardening, which was confirmed by taking microhardness measurements on axial cross-sections of the microtruss struts (an average of 36 ± 2 HV over all sample types using 0.98 N applied load and 10 s dwell time).

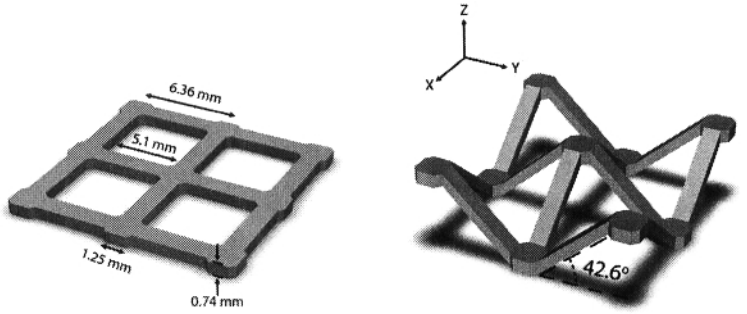

(a) (b)

Fig. 1. Schematic diagram of a starting perforated aluminum sheet (a) and the final architecture after forming (b).

The AA3003 pyramidal microtrusses were then subjected to three surface cleaning processes (degreasing, etching, and de-smutting) followed by hard anodizing to form a 40 μm thick anodic aluminum oxide coating on the surface of the microtruss cores. Samples were rinsed with de-ionized water between each step and after hard anodizing. Table I summarizes the process conditions for each step. The microhardness of the anodized coating was 537 ± 38 HV (using 0.98 N applied load and 10 s dwell time). Coated and uncoated (only subjected to surface cleaning) samples were then tested in uniaxial compression at a cross-head displacement rate of 1 mm/min using confinement plates that restricted the nodal displacement in the microtrusses. In addition, four coated samples were partially compressed to different strain level (starting from ε = 0 to ε = 0.53). The axial cross-sections of their internal struts were characterized by scanning electron microscopy (SEM).

Table I. Surface Cleaning and Hard Anodizing Specification

Process Name	Solution	Time	Temperature	Current density
Degreasing	5g/l Na_2CO_3 5g/l Na_3PO_4	10 min	87 ± 5°C	-----
Etching	5wt% NaOH	2 min	57 ± 2°C	-----
De-smutting	20vol% HNO_3	1 min	33 ± 2°C	-----
Hard anodizing	12wt% H_2SO_4 1wt% $(COOH)_2$	45 min	10 ± 1°C	4 A/dm^2

Results and Discussion

Figure 2 presents typical compressive stress-strain curves of the coated and uncoated samples. Both samples exhibit an initial elastic region (of slope E) before reaching a peak stress (σ_{peak}) that is followed by post-peak softening until a valley stress (σ_{valley}), and eventually final densification is reached.

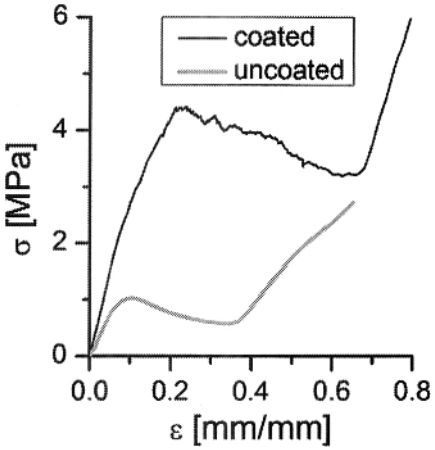

Fig. 2. Typical compressive stress-strain curves of the coated and uncoated microtrusses.

Figure 3 plots the slope of the stress-strain curve as a function of strain for both sample types. At a low strain level, both the coated and uncoated microtrusses elastically deform with nearly constant compressive modulus. After a strain of about $\varepsilon = 0.05$, the samples begin to deform plastically and the moduli values decrease, eventually dropping below zero. In the case of the uncoated samples, the modulus drops gradually to zero; the first x-intercept is the strain when the peak strength is recorded (ε_{peak}) while the second x-intercept is the strain when the valley strength is recorded (ε_{valley}). In the case of the coated samples, the local modulus passes through large oscillations as it progressively decreases; the first x-intercept is lower than the value of the ε_{peak} while the last x-intercept is higher than the value of the ε_{valley}. These modulus fluctuations indicate that the coated microtrusses are subjected to series of fracture events as they collapse, which is not commonly seen in the inelastic buckling of conventional microtrusses.

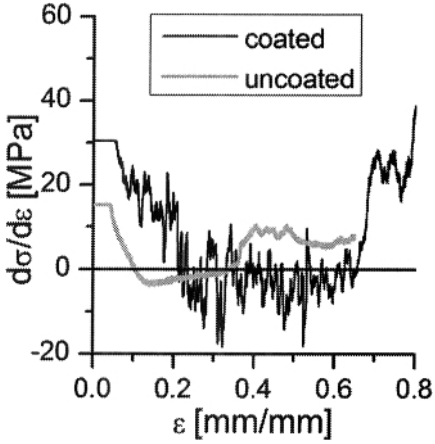

Fig. 3. Modulus ($d\sigma/d\varepsilon$) curves of the coated and uncoated microtrusses.

The energy absorption properties of the microtrusses can also be examined by measuring the area under their stress-strain curves (starting from half the peak stress to twice the peak stress, after [15]):

$$J_{densification} = \int_{\varepsilon\left(\frac{1}{2}\sigma_{peak}\right)}^{\varepsilon(2\sigma_{peak})} \sigma d\varepsilon \qquad (1)$$

The compressive properties of the coated and uncoated microtrusses are summarized in Table II. It seems at first surprising that with only a 40 μm thick anodized coating, the coated microtrusses were twice as stiff, four-times as strong, and had six-times the energy absorption capability of the uncoated microtrusses. Note that the post-peak softening region (defined as the difference between ε_{peak} and ε_{valley}) of the coated samples is 57% higher than that of the uncoated samples. Prolonging the post-peak behaviour while maintaining a high stress level is the key reason why the coated microtrusses have superior energy absorption characteristic.

Table II. Compressive Properties of the Coated and Uncoated Microtrusses.

Sample	E [MPa]	σ_{peak} [MPa]	ε_{peak} [mm/mm]	σ_{valley} [MPa]	ε_{valley} [mm/mm]	$J_{densification}$ [MPa]
Coated	33	4.20	0.26	3.19	0.62	2.96
Uncoated	15	1.03	0.1	0.58	0.33	0.50

Macroscopic Failure Mechanism

While the uncoated AA3003 microtrusses follow a conventional inelastic buckling collapse mechanism, the coated microtrusses fail in a very different manner. Backscatter scanning electron microscopy (figure 4) shows the evolution of the coated axial cross-sections of the coated microtrusses (x-direction in figure 1b) after different levels of compressive strain: $\varepsilon = 0$ (a), $\varepsilon = 0.24$ (b), $\varepsilon = 0.33$ (c), $\varepsilon = 0.44$ (d), and $\varepsilon = 0.53$ (e). The left-hand side of the as-coated sample (figure 4a) shows that the top part of the node is flattened due to the fabrication pin-indentation while the bottom part has a convex curvature, creating a region with a smaller cross-sectional thickness between the node and the strut. At $\varepsilon = 0.24$ (figure 4b), the microtruss is compressed closed to its peak strength. The bottom part of the node is now flattened due to compression and the top part is bulged outward. On the right-hand side closer to the node, a series of oxide pulverizations is seen, which explains the modulus fluctuation of the coated sample (figure 3). At strain-levels beyond the peak strain ($\varepsilon = 0.33$, 0.44 and 0.53), pulverization continues from the edge of the node, expanding along the strut length. Figure 5 shows the axial cross-sectional thickness of the core for each of these strain-levels along the length of the strut. For strain values greater than the initial peak strain of $\varepsilon = 0.26$, the samples show that the axial cross-section thickness first decreases to a minimum at the edge of the node, then increases within the pulverized region before decreasing again to the thickness level seen in the undamaged region of the strut. It is interesting to note that the strut remained at an angle of ~40° (near the starting angle of $\theta = 42.6$) throughout the collapse sequence. The fact that the undamaged segments of the struts retain nearly the same angle throughout collapse is one of the contributing factors to the prolonged post-peak behaviour of the coated microtrusses.

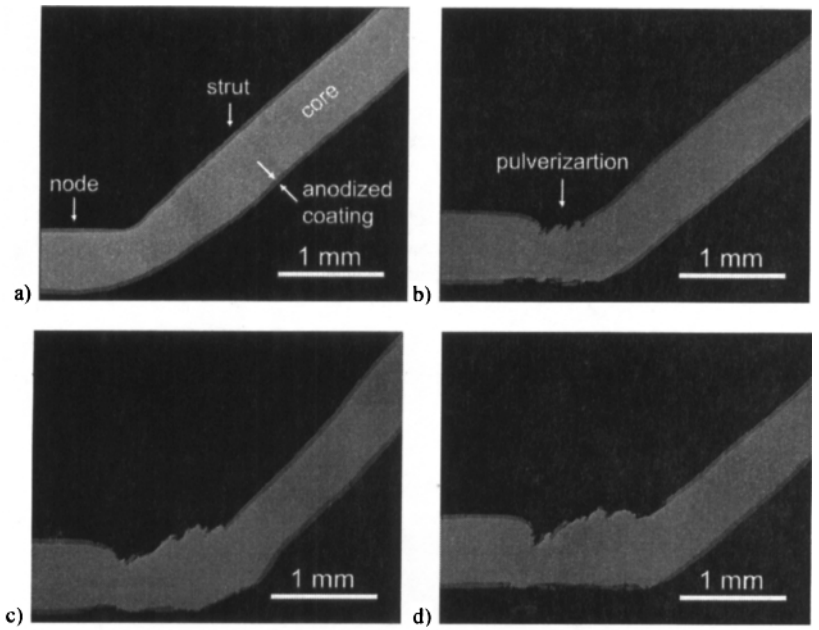

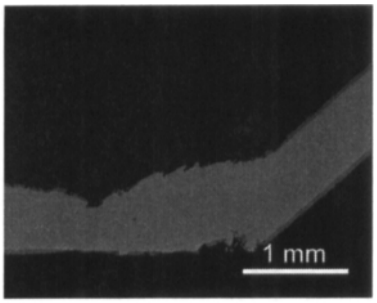

e)

Fig. 4. Backscatter scanning electron micrographs of the coated microtrusses at compressive strains of $\varepsilon = 0$ (a), $\varepsilon = 0.24$ (b), $\varepsilon = 0.33$ (c), $\varepsilon = 0.44$ (d), and $\varepsilon = 0.53$ (e).

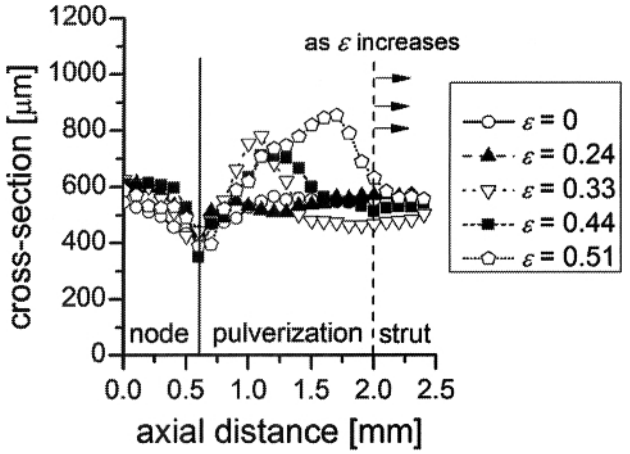

Fig. 5. Axial cross-sectional thicknesses of coated microtrusses cores at different strain levels starting from the centre of the node at increment of 100μm.